Food Hydrocolloids 144 (2023) 108987

Contents lists available at ScienceDirect

Food Hydrocolloids

journal homepage: www.elsevier.com/locate/foodhyd

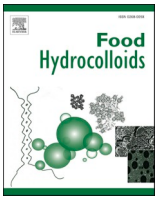

Designing bilayered composite films by direct agar/chitosan and citric acid-crosslinked PVA/agar layer-by-layer casting for packaging applications

Cherif Ibrahima Khalil Diop [a,*], Sagrario Beltran [a], Maria-Teresa Sanz [a], Javier Garcia-Tojal [b], Miriam Trigo-lopez [c]

[a] Department of Biotechnology and Food Science (Chemical Engineering Section), Faculty of Science, Universidad de Burgos, Pza. Misael Bañuelos S/n, 09001, Burgos, Spain
[b] Department of Chemistry (Inorganic Chemistry Section), Faculty of Science, Universidad de Burgos, Pza. Misael Pza. Misael Bañuelos S/n, 09001, Burgos, Spain
[c] Departament of Chemistry (Organic Chemistry Section), Faculty of Science, Universidad de Burgos, Pza. Misael Bañuelos S/n, 09001, Burgos, Spain

ARTICLE INFO

Keywords:
Double-layered films
Composite packaging
Agar/chitosan
Crosslinked PVA/Agar
Layer-by-layer casting

ABSTRACT

Packaging is a crucial tool for reducing food waste and enhancing product competitiveness. Fossil fuel-based plastics, mostly used for food packaging, account for nearly 40% of global plastic waste. To address this issue, this study developed a layer-by-layer casting technique to create novel bilayered plastic composites with distinct agar/chitosan and PVA/agar layers. Film's properties, such as thickness, plasticity, and tensile strength, were affected by adjusting the volume of the layers. The elongation at break was positively related to the presence of citric acid (up to 30 wt%) as a crosslinker. The chitosan-rich first layer provided better UV-light blocking potential and opacity, which were beneficial in the prevention of lipid oxidation. Increasing the second layer by 40–60% substantially reduced the light absorption, while the colors were proportional to the citric acid content. The FT-IR band at 1713 cm^{-1} indicated an increase in C=O ester groups with crosslinker content. The hydrophobicity of the films was enhanced by the chitosan-rich layer. XRD supported intramolecular and intermolecular hydrogen bonding, whereas the micrographs revealed tightly bound structure between layers. The results corroborated that the inclusion of agar in the formulations increased the stability of the film, making it ideal for various packaging applications.

1. Introduction

Globally, an estimated volume of 1.3 GTonnes of food is wasted annually, according to the United Nations Food and Agriculture Organization (FAO). 13.8% of the food produced is wasted at the upstream stages of the food supply chain: retail and consumer (FAO, 2019). Packaging is critical in protecting the material from tempering and any kind of physical, chemical, and biological contamination, particularly in the food industry. Therefore, food packaging has become an essential tool for the reduction of food waste and increasing food competitiveness. Its action is closely related to the extension of the shelf life, particularly for minimally processed foods, resulting in a non-negligible contribution to a lower environmental impact (Brennan et al., 2021). Additional roles consist of offering visibility to packed products and facilitating their distribution, marketing, and safe use (Sonneveld, James, Fitzpatrick, & Lewis, 2005).

Fossil fuel-based materials such as plastic are among the most used materials for food packaging (Mohanty & Swain, 2017) and generate around 40% of global plastic waste (OECD, 2022).

However, negative perceptions and concerns about plastic are growing among consumers and governments. These relatively cheap, light, and malleable materials with good processing capability persist following product consumption, generating waste that has become an urgent environmental issue (Brennan et al., 2021). The most common used waste management strategies refer to the reduction, re-use, recycling, and recovery of this kind of waste. Most plastic is too expensive to recycle, we incinerate six times as much plastic as we recycle, and over 90% of the plastic ever made has not been recycled (Greenpeace, 2022). The urgent need to make the lifecycle of plastics more circular calls for an expansion of national policies and improved international

* Corresponding author.
E-mail address: cidiop@ubu.es (C.I.K. Diop).

https://doi.org/10.1016/j.foodhyd.2023.108987
Received 24 March 2023; Received in revised form 2 June 2023; Accepted 17 June 2023
Available online 26 June 2023
0268-005X/© 2023 The Authors. Published by Elsevier Ltd. This is an open access article under the CC BY-NC-ND license (http://creativecommons.org/licenses/by-nc-nd/4.0/).

cooperation to mitigate environmental impacts all along the value chain (OECD, 2022).

Packaging manufacturing generated in the EU a turnover of EUR 355 billion in 2018, with waste management operators generating EUR 15 billion. The total packaging waste generation is expected to rise from 78 million metric tons in 2020 to 92 million metric tons in 2030, and 107 million metric tons in 2040. The European Commission's packaging waste Directive 94/62/EC proposes reducing the negative environmental impacts of packaging and packaging waste. One of its specific objectives is to promote the circular economy for packaging in a cost-effective way. The measure promotes a reduction of the fossil fuel requirements of the EU by 3.1 million tons per year (almost 1/4 of the fossil fuel needed currently for plastic packaging production) (European Commission, 2022).

Recent strategies have focused on the development of biodegradable materials for use as environmentally friendly food packaging and coating. As a part of green strategies fixed in the UN 2030 agenda for sustainable development goals, this field provides hot, challenging topics in research and development (Lee et al., 2016).

Biobased plastics, for instance, include biodegradable materials generated from natural and synthetic biopolymers from renewable resources. A comparison must be made between biobased plastics, as some materials such as biopolyethylene, bio-polypropylene, and bio-polyethylene terephthalate (PET) do not offer a better end of life due to their lack of biodegradability (Rahman & Bhoi, 2021). Non-biodegradable bioplastics represent 57% of all bioplastics, with partially biobased polyethylene terephthalate currently leading the market, followed by biobased polyamides and fully biomass-derived polyethylene (Andreeβen & Steinbüchel, 2019).

Various natural biopolymers, including but not limited to starch (Thakur et al., 2019), chitosan (Mujtaba et al., 2019), and alginate, are abundant in nature, biodegradable, and have proven film forming capabilities. When used individually they present a certain number of limitations in relation to poor barrier, mechanical properties, and processability, as compared to petroleum-based polymers (Wu et al., 2017). Strategies such as biopolymer blending (Basumatary, Mukherjee, Katiyar, & Kumar, 2022), structural modification (Ojogbo, Ogunsona, & Mekonnen, 2020; Diop, Li, Xie, & Shi, 2011) as well as compounding with synthetic polymers and or minerals, have all been found to be effective strategies that extend their application by overcoming these technological drawbacks (Wu et al., 2017).

On the other hand, multilayered food packaging has revolutionized the food packaging industry in terms of barriers, safety, handling, printing, and mechanical requirements. It consists of a superposition of at least two layers, one covering the other (Le Gars et al., 2020). Multilayer plastic films are widely used as industrial packaging for food protection, principally fruit and vegetables, representing 26% of the packaging market (Wagner, 2016). In conventional multilayered packages, each layer plays a complementary role vis-a-vis the rest of its counterparts. Their inhomogeneity is one of their major limitations. Adhesion between distinct layers and lack of biodegradability render the whole package hardly recyclable (Diop, Lavoie, & Huneault, 2017).

Layer-by-layer deposition, electrodynamic processing, microlayer coextrusion along with bar coating are among the most used techniques for building multilayered materials (Le Gars et al., 2020). Similarly, Hosseini, Javidi, and Rezaei (2016) prepared multilayered films based on PLA and fish gelatin by successive solvent-casting procedures, with oxygen and water vapor barrier properties enhanced by 87 and 91%, respectively, compared to pristine PLA.

Polyvinyl alcohol (PVA) is a highly attractive polymer due to its low cost, food friendly, tunability, transparency, and film forming capacities. It is a versatile candidate for replacing fossil-based plastic films for food applications. Because it is highly hydrophilic, its advantages are lowered by its low barrier properties, and its blending with biopolymers results in multiphasic systems able to overcome some limited functionalities. On the other hand, citric acid, as an effective crosslinking agent, improved the blend homogeneity between PVA and other biopolymers such as starch. The production of a compact bulk morphology tends to improve the properties of composite materials (Jose & Al-Harthi, 2017).

Therefore, in this study, a layer-by-layer approach through solvent casting has been used to develop bilayered biocomposite films made up of a layer of agar-chitosan covered with a citric acid crosslinked agar/PVA blend layer. Fig. 1 shows the structural composition of chitosan, polyvinyl alcohol, and agar (agarose) molecules. Chitosan is a linear polycationic polysaccharide composed of repeating units of glucosamine (Fig. 1-a) and *N*-acetylglucosamine, derived from the deacetylation of chitin (Jayakumar et al., 2010). The degree of deacetylation varies depending on the source of the material and the processing method. PVA is a synthetic linear polymer of vinyl alcohol (Fig. 1-b) made by the polymerization of vinyl acetate, followed by hydrolysis of the resulting polymer to remove acetate groups. Agar (Fig. 1-c) is a complex polysaccharide composed of a repeating unit of agarose and agaropectin linked by hydrogen bonding (Diop, Trigueros, Sanz, Beltran, & García-Tojal, 2022). The structure of agarose consists of alternating residues of D-galactose and 3,6-anhydro-L-galactose, while agaropectin contains additional branching and sulfation patterns. Following process optimizing, the multiphase materials were characterized in terms of physical, and mechanical properties.

2. Material and methods

2.1. Materials

Agar powder and citric acid (99.99%) were purchased from VWR (Leuven, Belgium). High molecular weight chitosan (>75% deacetylated, Mw = 310.375 KDa), fully hydrolysed polyvinyl alcohol (Mw app. 145,000), and glycerol 99.5% were supplied by Merck (Darmstadt, Germany).

2.2. Methods

2.2.1. Preparation of the double layered film

A direct layer-by-layer deposition approach through solvent casting was used to prepare the double layer film (Zhao et al., 2020). Therefore, a first layer made from a blend solution of agar and chitosan was surrounded by a layer made from a mixture of agar, polyvinyl alcohol (PVA), and citric acid. The manufacturing process of the bilayered composite films has been displayed in Fig. 2.

2.2.2. Preparation of the film forming solutions

2.2.2.1. Preparation of the agar/chitosan blend solution. Agar powder was dissolved in distilled water in the presence of glycerol (30% of the agar dry weight) as a plasticizer in a 500 mL double-wall glass reactor (Alamo, Madrid, Spain) connected to a heated recirculating thermostat (JP Selecta, Barcelona, Spain). The agar suspension (1.5% w: v) was heated for 3 h at 85 ± 5 °C under stirring at 300 rpm using a Teflon stir bar. The hot agar solution was then filtrated using a double layered cheese cloth to remove impurities or undissolved particles.

Concomitantly, a 1.5% (w: v) chitosan solution was separately prepared by dissolving the chitosan in 2% acetic acid at 75 ± 5 °C for 3 h in the presence of plasticizer (glycerol, 30% dry weight) using a 500 mL double-walled glass reactor installation as previously described. Chitosan dissolution was carried out under vigorous stirring at 300 rpm using a stir bar. The resulting chitosan solution was then filtered through a double layer of cheesecloth.

To prepare the blend solution, the chitosan solution has been mixed with the agar solution in the reactor at a 35: 65 (% v: v) percent ratio under vigorous stirring (400 rpm). The mixture was then heated to 75 ± 5 °C for an hour and then left at that temperature without stirring for at least 30 min to remove bubbles.

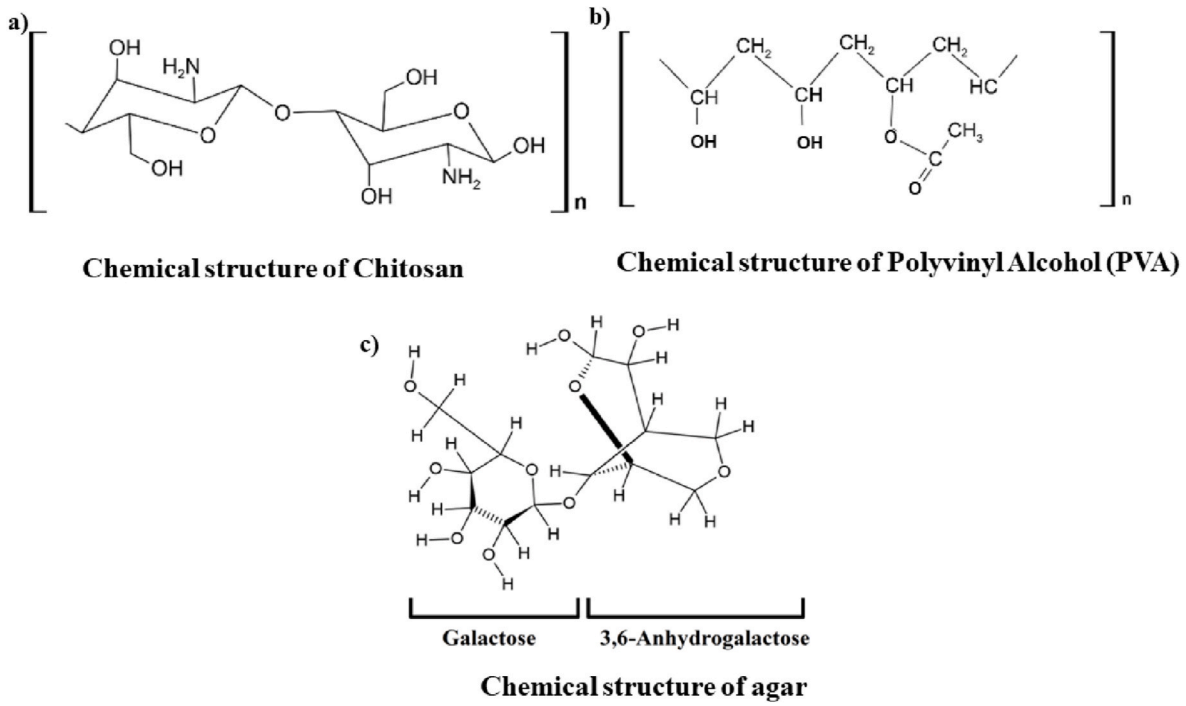

Fig. 1. Chemical structure of a) chitosan, b) Polyvinyl alcohol (PVA) and c) agar.

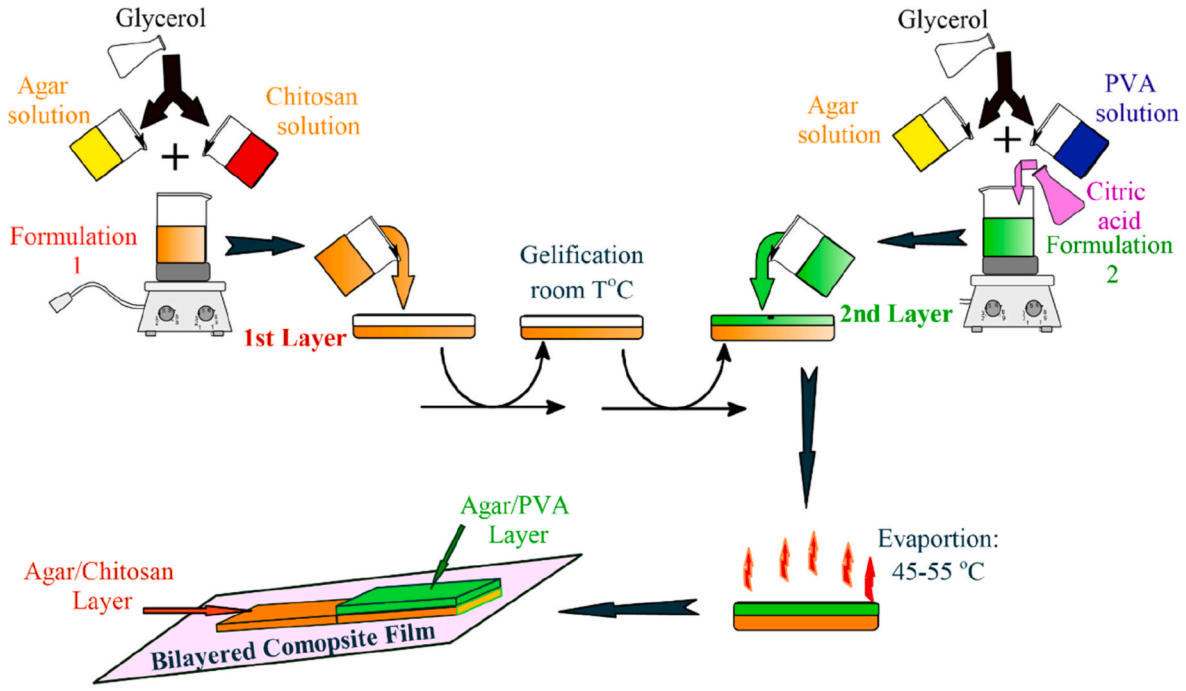

Fig. 2. Preparation scheme of the agar/chitosan-agar/PVA double layered composite films.

2.2.2.2. Preparation of the PVA/agar blend solution. PVA pellets were dissolved in distilled water with 30% (dry weight) glycerol to form a 5% (w: v) solution. Citric acid at different concentrations (from 0 to 30% of the PVA dry weight) was added to the solution as a crosslinking agent. The solution was then heated at 90 ± 5 °C under vigorous stirring (300 rpm) for 2 h, or until a clear, transparent, and homogeneous solution was obtained.

The agar/PVA blend solution was prepared by mixing the glycerol-plasticized agar solution (as earlier prepared) and the glycerol-plasticized crosslinked PVA solution at a 35: 65 (% v: v) percent ratio. The blend solution was mixed at 90 ± 5 °C for an hour at 300 rpm and the homogeneous liquid solution was then left unstirred for an additional hour at this temperature to remove bubbles.

2.2.2.3. Preparation of the double layered composite films. The first layer of the film was prepared by casting a predefined volume of the agar/chitosan blend solution onto a 10 cm diameter, leveled Teflon plate. Due to the thermo-reversibility of the agar structure, the casted solution was allowed to gel at room temperature for 20 min. The solidified agar/

chitosan blend solution was then surrounded by a layer of the PVA/agar/citric acid blend solution on its top and allowed to stand at room temperature for another 20 min. The double layered films were formed by evaporating the solutions for 36 h at 45 ± 5 °C in an air circulating oven. Other film specimens were prepared by drying the layer-by-layer casted solution at higher temperature of 55 ± 5 °C. The appropriately dried film was peeled off, put in a Ziploc, and placed in a desiccator with a $Mg(NO_3)_2$ saturated solution (53% RH) for 7 days prior to testing. By adjusting the volume of the respective casting solutions, the variation of the proportion of each of the 2 layers in the films was optimized. Table 1 displayed the different films' formulations as well as their thickness and color.

The thickness of the obtained double layered films was measured using a RS Pro digital thickness gauge with a resolution of 0.01 mm (RS, Manchester, UK) at six random different points around the film.

The moisture content of the composite double layered films has been measured using a moisture analyzer (MB 120, Ohaus, New jersey, USA). About 1 g (to near 0.0001 g) of the sample was heated using halogen heating at 105 °C until complete water evaporation (about 15 min).

The water uptake and thickness swelling of the composite films were measured by soaking the specimen in distilled water at room temperature. The weight and thickness were measured every hour for 24 h and recorded after being thoroughly dewatered. All specimens were measured in triplicate, and water uptake (%) and thickness swelling were determined following Eqs. (1) and (2).

$$Water\ uptake\ (\%) = \frac{W_0 - W_1}{W_0} \times 100 \quad (1)$$

Where W_0 and W_1 are the initial and final dried weight of samples, respectively (Wang et al., 2017).

$$\text{Thickness swelling}\ (\%) = \frac{T_0 - T_1}{T_0} \times 100 \quad (2)$$

Where T_0 and T_1 are the initial and final thickness of the samples, respectively.

2.2.3. Surface color analysis

The L*, a*, and b* color values of the unlayered and bilayered films were measured by a Hunter LAB colorimeter (Hunterlab, Reston, VA). The colorimeter was standardized with a white reflectance standard tile and a black tile. The same white tiles served as a background for the color analysis. The lightness coordinate (L*) measures how much light is reflected (100 = all light reflected; 0 = all the light absorbed), a* (positive values indicate the red color, while negative values indicate the green color) and b* (positive values denote the yellow color and negative values denotes the blue color). Measurements were performed at five distinct random points perpendicular to the film surface for each sample. The means L*, *a**, *b** values were obtained from triplicate analysis.

2.2.4. Light barrier properties of the composite films

The light barrier properties of the double layered composite films have been determined by measuring the transmittance of the samples at wavelengths between 200 and 800 nm using a spectrophotometer V-670 (Jasco, Japan). The tests were carried out in the transmittance mode by placing a film between two the walls of a UV-quartz cuvette as sample holders. Measurements were determined using air as a blank.

$$transparency = \frac{(log\%T600)}{x} \quad (3)$$

where $\%T_{600}$ is the percent transmittance at 600 nm and x is the film thickness (mm). The opacity of the films was calculated from the absorbance at 600 nm, following Eq. (4).

$$Opacity = \frac{Abs_{600}}{x} \quad (4)$$

where Abs_{600} is the absorbance at 600 nm and $x$is the film thickness (mm).

2.2.5. Mechanical properties of the films

The mechanical properties, such as the tensile strength (TS), Young's modulus and elongation at break (E) of the composite films, were

Table 1
Formulation, thickness, and color evaluation of the agar/chitosan - PVA/agar double layered composite films.

Film's code	Film's formulation				Thickness (mm)	Moisture (%)	Color coefficients		
	Agar/Chitosan volume (%)	Agar/PVA volume (%)	Citric acid (%)	Glycerol (%)			L*	a*	b*
CAPA10	100	0	0	30[c]	0.15 ± 0.01	7.48 ± 0.81	79.44 ± 1.9	−1.58 ± 0.39	32.45 ± 3.3
CAPA64	60	40	15[b]	30 [c]	0.21 ± 0.03	5.23 ± 0.33	74.64 ± 0.8	0.07 ± 0.30	33.53 ± 1.9
CAPA55	50	50	15 [b]	30 [c]	0.23 ± 0.03	3.65 ± 0.46	75.33 ± 1.8	−0.55 ± 0.27	19.28 ± 2.1
CAPA46	40	60	15 [b]	30 [c]	0.26 ± 0.02	3.49 ± 0.40	79.04 ± 2.3	−0.68 ± 0.50	15.97 ± 3.1
CAPA01	0	100	15 [b]	30 [c]	0.32 ± 0.07	4.23 ± 0.76	81.13 ± 2.3	0.815 ± 0.03	−5.13 ± 0.06
CAPA55–0	50	50	0	30 [c]	0.20 ± 0.05	4.66 ± 0.55	67.59 ± 3.0	0.35 ± 0.73	28.00 ± 7.6
CAPA55–5	50	50	5 [b]	30 [c]	0.28 ± 0.03	4.00 ± 0.62	77.87 ± 2.5	−1.62 ± 0.07	12.50 ± 2.4
CAPA55–30	50	50	30 [b]	30 [c]	0.33 ± 0.04	3.60 ± 0.39	80.74 ± 0.1	−1.04 ± 0.32	10.80 ± 0.8
CAPA55-5-T5 [a]	50	50	5 [b]	30 [c]	0.24 ± 0.04	4.01 ± 0.34	65.09 ± 3.4	−2.77 ± 0.19	17.83 ± 2.1
CAPA55–15-T5 [a]	50	50	15 [b]	30 [c]	0.23 ± 0.02	3.64 ± 0.28	49.53 ± 0.5	15.025 ± 1.43	42.31 ± 0.7
CAPA55–30-T5 [a]	50	50	30 [b]	30 [c]	0.30 ± 0.03	3.59 ± 0.31	78.99 ± 0.5	−1.95 ± 0.05	19.26 ± 1.9

[a] Films dried using higher temperature of 55 °C. The rest of the films were dried at 45 °C.
[b] The citric acid (crosslinker) concentration in the formulation was related to the dry weight of the agar/PVA blend.
[c] The glycerol (plasticizer) concentration in the formulation was related to the dry weight of the total solid in each separate solution composing the blend layer's formulation.

evaluated using Shimadzu Compact Tabletop Testing Machine EZ Test universal tester (Shimadzu, Kyoto, Japan) operated in tensile mode with a 500 N load cell and a tensile crosshead speed of 10 mm/min. The preconditioned films were cut into 0.5 × 5 cm strips and placed between metallic grids with an initial gauge length of 3 cm after their average thickness was measured.

The stress-strain curves of the films were obtained using Trapezium X software (Shimadzu Corp., Kyoto, Japan) and the tensile strength (TS), elongation at break were deducted from the curves and expressed in MPa.

The Young's modulus (the force per unit area) was calculated directly from a Trapezium X (Shimadzu, kyoto, Japan) data acquisition software from the slope of the tensile stress-deformation curve using an offset-yield approach in the initial linear elastic region of the curve. The TS was directly determined from the software by dividing the maximum load (N) by the initial cross-sectional area (m^2 of the films based on the gauge dimensions and specific thickness of each specimen) and expressed in MPa.

$$T_{S=}\frac{F}{S} \tag{5}$$

Where TS is the tensile strength (MPA), F (N) is the maximum tensile force when the sample breaks and S (m^2) is the cross-sectional area of the specimen.

At least five replicates were carried out for each film specimen.

2.2.6. Fourier transform infrared analysis (FT-IR)

The structural interaction between molecules in the composite double layered film has been analyzed using an FT-IR (Jasco FT-IR 4200) equipped with an attenuation total reflection (ATR) using a diamond crystal (Jasco Corporation, Tokyo, Japan). The spectra were collected using Spectra Manager, version 2 (JASCO Corporation, Tokyo, Japan) at a frequency of 62 scans and a resolution of 4 cm^{-1} in the range 4000 to 400 cm^{-1}.

2.2.7. Thermogravimetric analysis (TGA)

The thermal stability of films was evaluated using a thermogravimetric analyzer (Q50, TA Instruments, Water LLC, New Castle, Delaware, USA). About 25 mg of film sample was taken in a standard aluminum cup and heated from 25 to 550 °C with a heating rate of 10 °C/min under a nitrogen flow of 20 mL/min. An empty cup was taken as a reference.

2.2.8. X-ray diffraction (XRD) analysis of the films

The X-ray patterns of the bilayered composite films were characterized using an X-ray diffractometer (D8 Discover Davinci, Bruker AXS GMBH) with Cu Kα radiation at a voltage of 40 kV and 30 mA. The diffraction angle was set in the range of 2θ = 10 and 80°, with a scanning speed of 2° min^{-1}. The preconditioned films were dried prior to testing.

2.2.9. Scanning electron microscopy (SEM)

The surface and cross-sectional microstructure of the composite films were observed using an SEM (JSM–6460, JEOL Ltd., Japan) operated at 10 kV. The cross-sections of the films were exposed after being cut with a sharp cutting tool. The films were fixed with conductive adhesive and conductive gold was sputtered on the specimen prior to their observation. The observation was carried out at different magnifications.

2.2.10. Statistical analysis

All experiments were performed in triplicate, and the average values were calculated, including their standard deviations. Data were collected and analyzed at an ANOVA significance level of 5% (p 0.05). Microsoft Excel 365 and Statgraphics Centurion 19 (Statgraphics Technologies) software were used for all analyses, including Pearson Moment correlation.

3. Results and discussion

3.1. Film moisture content and thickness

Moisture content is associated with the presence of water molecules in the network microstructures of the films. Table 1 shows the moisture content values of unlayered and bilayered composite films. The unlayered CAPA10 composite film was found to have higher water content that its CAPA01 counterpart. As a result, creating double layered films and the increasing the second agar/PVA/citric acid layer resulted in a reduction of the moisture content. Wahyuningsih, Iriani, and Fahma (2016) founded moisture content value of 6.03% for pure PVA control film. Table 1 also showed that the use of citric acid as crosslinker agent appears to reduce the residual film moisture content. On the other hand, drying the films at higher temperature (55 °C) seemed not to have an impact on the moisture content at a specific citric acid concentration. As also observed by Park, K., Oh, Y., Panda, P. K., & Seo, J. (2022), the presence of crosslinking lowers the availability of OH groups and acts as a barrier to penetrate through the tightly crosslinked network structure of the film.

Fig. 3 displays the image of the double layered composite films prepared from the two different agar-based formulations. The thickness of the composite films was influenced by the film forming procedure, which in turn affected their mechanical characteristics. In contrast to the thinner unlayered films resulting from the CAPA10 formulation, the CAPA01 formulation, formed thicker unlayered films. The superposition of different volumes of these two fractions altered their respective thicknesses in the designed double layered composite materials. Increasing the volume of the second PVA/agar layer correspondingly increased the film thickness. On the other hand, the crosslinking effect of citric acid in the PVA/agar second layer influenced the thickness values of the bilayered films. The higher the citric acid content in the formulation (from 0 to 30%), the thicker the resulting composite films, as shown in Table 1. In contrast, the drying temperature did not show a noticeable impact on the double layered composite films' thickness.

3.1.1. Color L*, a*, b*

The three CIELAB coordinates L* (lightness), a* (green to red), and b* (blue to yellow) were used to evaluate the color variation of the double-layered composite films as a function of their respective compositions. The colorimetric values were summarized in Table 1. High L* values exceeding 60 were obtained for the evaluated films that indicated a predilection towards whiteness (L* = 100). The unlayered CAPA01, which was characterized by the predominance of PVA solution over the agar solution had the highest L* values, followed by CAPA10, which was exclusively made of a single layer of a chitosan and agar blend. The addition of the second crosslinked PVA/agar layer appeared to reduce the lightness values of the bilayered films in comparison to CAPA10 until a volume equilibrium between the two layers was achieved (ratio 1:1 v: v). A further increase of the second layer's volume in the composition led to an augmentation of the film's lightness value. PVA typically produces films with high levels of transparency and lightness (Haghighi et al., 2021), therefore, its dominance in the films as a result of the expansion of the second layer's fraction, inherently impacted the overall L* values. The presence of citric acid as a crosslinker between PVA and other biopolymers in the formulation had a favorable impact on the bilayered films' lightness, which increased with an increase in the citric acid concentration from 0 to 30%. Similar observations have been reported by Uranga, Nguyen, Si, Guerrero, and De la Caba (2020) for crosslinked agar/fish gelatin films. Moreover, the unlayered PVA/agar films demonstrated a strong propensity to redness and blueness (a* = 0.81, b* = −5.13), in contrast to the CAPA10 (a* = −1.58, b* = 32.45), which tended towards more greenish and yellowish colorations. The lower a* value of the latter films might be primarily attributed to the preponderance of agar over the chitosan fraction in the blend, as a similar observation has also been affirmed by Agusman Fransiska et al.

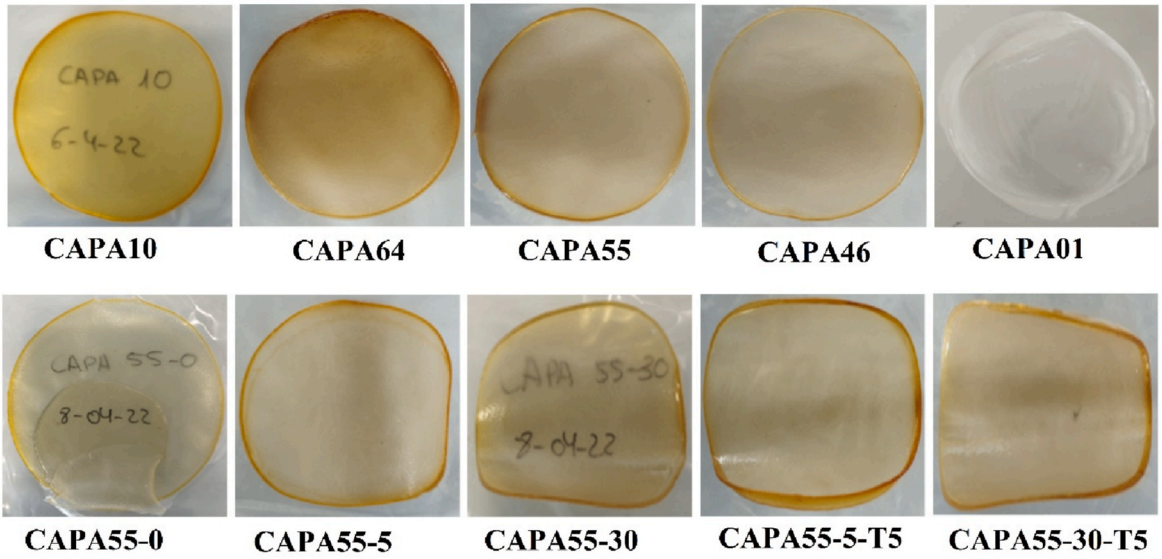

Fig. 3. Image of the agar/chitosan – PVA/agar double layered composite films at different volume concentrations.

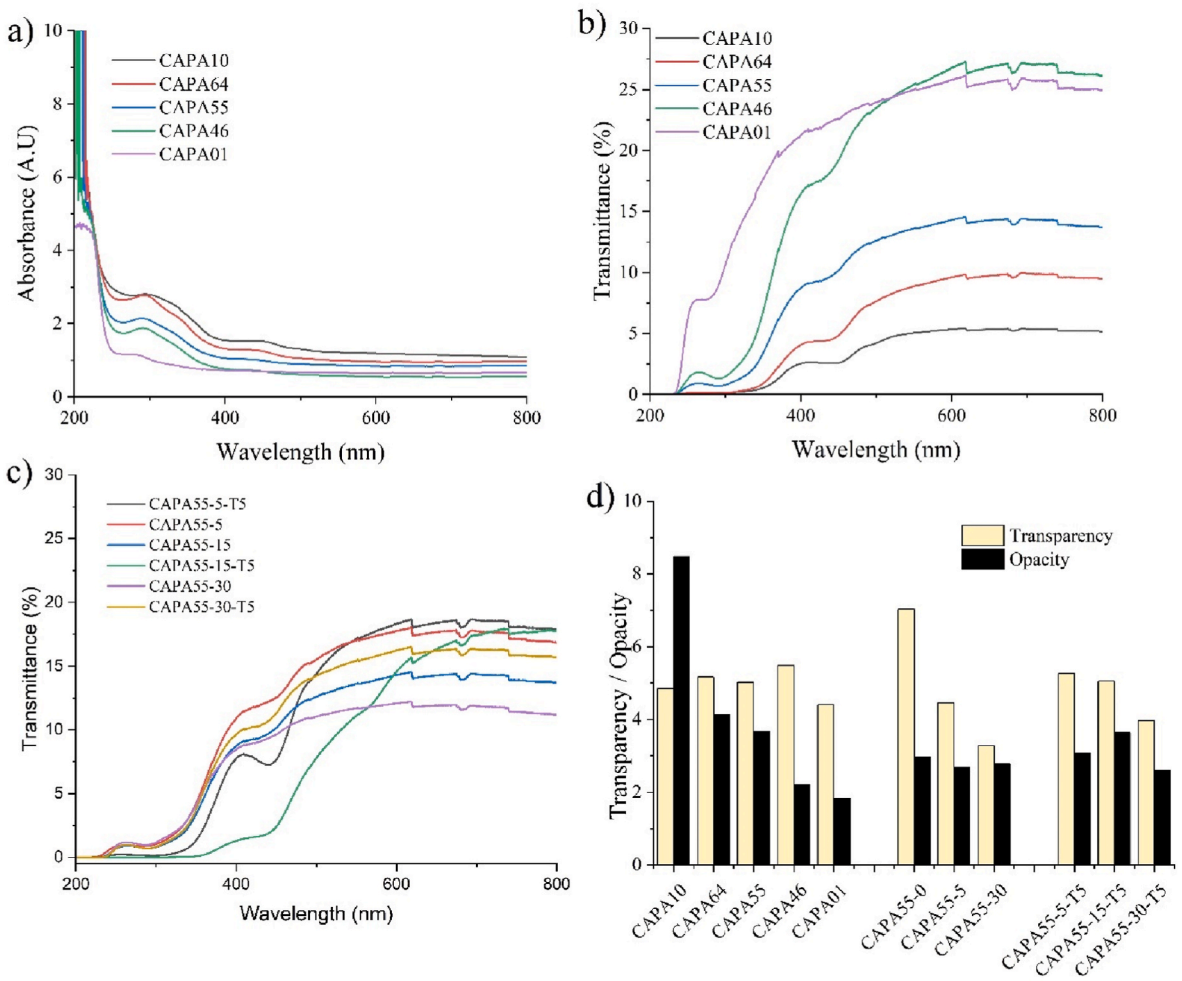

Fig. 4. a) UV-absorbance of the bilayered film in function of the layer's volume's variation. b) UV-Transmittance of the bilayered film in function of the layer's volume variation. c) UV-Transmittance of the bilayered film in function of the citric acid concentration and drying temperatures. d) Transparency and opacity of the different bilayered composite films.

(2022). In other terms, increasing the volume of the PVA-rich second layer in the formulation mitigated the color appearance of the bilayered films. Moreover, except for the CAPA-15-T5 that unpredictably displayed a higher a* and b* values, the increase of the citric acid crosslinking agent, especially in these double layered composite films, was accompanied by a decline of both the reddish and yellowish colors, which were proportional to the citric acid content (Table 1).

3.2. Light transmittance

The light transmission parameters of the double layered composite films were evaluated to determine their impact against light protection, particularly UV radiations. Fig. 4 depicts the percent absorbance (Fig. 4-a) and transmittance (Fig. 4-b-c) of the different films when subjected to radiation ranging from 200 to 800 nm, as well as their transmittance and opacity values. Unlayered CAPA10 film made of an agar/chitosan blend plasticized with glycerol had the highest absorbance spectra in this wavelength range. The lowest absorbance was obtained when crosslinked PVA/agar occupied 100% of the film's volume (unlayered CAPA01). Consequently, the light absorption was significantly reduced when agar/chitosan was surrounded by a second layer of crosslinked PVA/agar at volumes ranging from 40 to 60% of the total film to generate the double layered films.

As a result, of the increased second layer percentage in the film, the area of the broad absorption band appearing between 230 and 320 nm was reduced. Adding the second layer also led to a drop in the peak intensity, from 3% for CAPA10 to 1% for CAPA01. It's worth mentioning that, depending on the film formulation, the peak of this latter band occurred at slightly varying wavelengths. The peak was, therefore, recorded at around 300 nm for CAPA10, 290 nm for the double layered films, and 280 nm for the unlayered CAPA01 film. CAPA10, CAPA64, CAPA55, and CAPA46 displayed an additional band at around 450 nm (Fig. 4-a). The intensity of this band, which was not detected for the CAPA01 film, decreased proportionally to the volume increase of the film's second layer and was therefore attributed to the presence of chitosan.

Fig. 4-b illustrates the percent transmittance of the films at increasing wavelengths. CAPA10 and CAPA64 displayed better UV barrier properties, around 100% (0% transmittance) in the 200–320 nm range (UV–C and UV-B regions). The wavelength range between 200 and 315 nm has been identified as the most susceptible region for phenomena such as lipid oxidation (Cazón, Vázquez, & Velazquez, 2019). In the higher UV region, the transmittance increased moderately to a maximum of 2.6 and 4% at 400 nm for CAPA10 and CAPA64, respectively. The total amount of the crosslinked PVA/agar's second layer in the films tended to gradually reduce their UV-blocking capacity. As expected, the unlayered CAPA01 had the lowest performance for blocking UV radiations, with transmittance of about 8% at 280 nm and 21% at 400 nm. This could be evidence that the presence of the first layer of chitosan/agar blend fostered an improvement of the UV barrier properties of the bilayered composite films. Overall, the low transmittance values in the UV region, combined with the improved visual appearance due to the presence of PVA in the visible region, may make these composites an excellent option for food active packaging applications. Their light-barrier properties could be suitable to prevent UV-light-induced lipid oxidation (Cazón et al., 2019). A higher drying temperature of 55 °C, on the other hand, appeared to significantly improve the UV blocking ability of the films in the presence of the crosslinking agent (5–15% citric acid) (Fig. 4-c). This phenomenon was particularly visible in the UV-C and UV-B regions, where the transmittance values were kept low in comparison to their counterparts dried at 45 °C. In the UV-A region, however, contrarily to the CAPA55-15-T5 (15% citric acid dried at 55 °C) film, which maintained similar barrier properties (%T ≈ 1% at 400 nm), the CAPA55-5-T5 with 5% citric acid exhibited a sudden rise in light transmittance to a maximum of approximately 8% at 400 nm (Fig. 4-c). CAPA55-5, CAPA55-15, and CAPA55-30 dried at 45 °C, however, did not show clear variations under 400 nm. They displayed higher tolerance to UV radiation as compared to their counterparts containing respectively 5 and 15% citric acid and dried at higher temperature, except for CAPA55-30-T5. Uranga et al. (2020) stated that temperature was an important crosslinking parameter for crosslinked film. However, the increase in the drying temperature seemed to improve the UV blocking capacity only at lower citric acid concentrations (Infurna, Cavallaro, Lazzara, Milioto, & Dintcheva, 2022).

When the films were exposed to visible light (radiations ranging from 400 to 800 nm), they displayed more complex behaviours, and increasing the drying temperature did not appear to favor better light blocking properties. It was nonetheless noticed that the higher the citric acid concentration, the better the light barrier properties of the double layered composite films. The crosslinking effect on the film when it dried at 45 °C led to lower transmittances in the visible region. Fig. 4-d displays the transparency and opacity of the films as determined from, respectively, the percent transmittance and absorbance at 600 nm. Low opacity values are generally required to obtain the best appearance properties. The unlayered films CAPA10 and CAPA01 had the lowest transparency values, while the bilayered films did not significantly improve the composite films' transparencies. Furthermore, when evaluating the impact of the citric acid content, it was established that higher film transparency was noticed for the films formulated without crosslinking agent (CAPA55-0). The transparency of the composite materials seemed to decrease proportionally as the citric acid concentration was increase to up to 30%. This could evidence a critical impact of the polymer crosslinking effect on films' transparencies, particularly at lower drying temperatures, as also evidenced by Lipatova and Yusova (2021). A higher drying temperature (55 °C) seemed to improve the transparency of the composite films when high citric acid content was involved. A reasonable explanation could be the cross-linking reaction between PVA and agar, on the one hand, and possibly between the first and second layers (throiugh citric acid migration), resulting in a more uniform and smoother surface structure of the films (Jiang et al., 2020).

Likewise, among the unlayered films, CAPA10 exhibited higher opacity as compared to CAPA01, which had the lowest opacity value. These made obvious the decrease in opacity noticed when these two formulations were combined to make the double-layered films. The opacity was, thus related to the volume of the second layer in the film. In contrast to the film transparency, the crosslinking effect of citric acid and the variation in the drying temperatures did not appear to have a considerable impact on the opacity parameters. However, reducing film lightness may help to prevent oxidative deterioration in packed foods caused by exposure to visible and UV light, which can result in nutrient losses, discoloration, and off-flavors (Uranga et al., 2020).

Overall, the bilayered composite films exhibited a good visual appearance associated with high transparency and low opacity. It is also probable that the presence of agar in both formulations facilitated the homogeneous interaction of both PVA and chitosan on both sides of the films and inside the matrix, modifying their optical properties.

3.3. FT-IR (ATR)

FT-IR-ATR was used to investigate the change in the chemical structure of the functional groups of the double layered composite films. Fig. S1 (Supplementary material) showed the FT-IR spectra of the films in function of the variation of the two layers 'ratios. Fig. 5(a–b) showed the FT-IR spectra of the different films made of an equal ratio of the two layers as a function of the temperature and citric acid content. The tested films showed a characteristic broad band located at around 3260 cm^{-1} (Fig. S1 as supplementary elements). This band, however, varied in intensity and area, perhaps due to the overlapping impacts of the different molecules present in the film formulation. Fig. S1 and Fig. S2 (as supplementary materials) showed that the most prominent bands in the IR spectra of CAPA01 and CAPA10 are noticed, with slight shifts in some

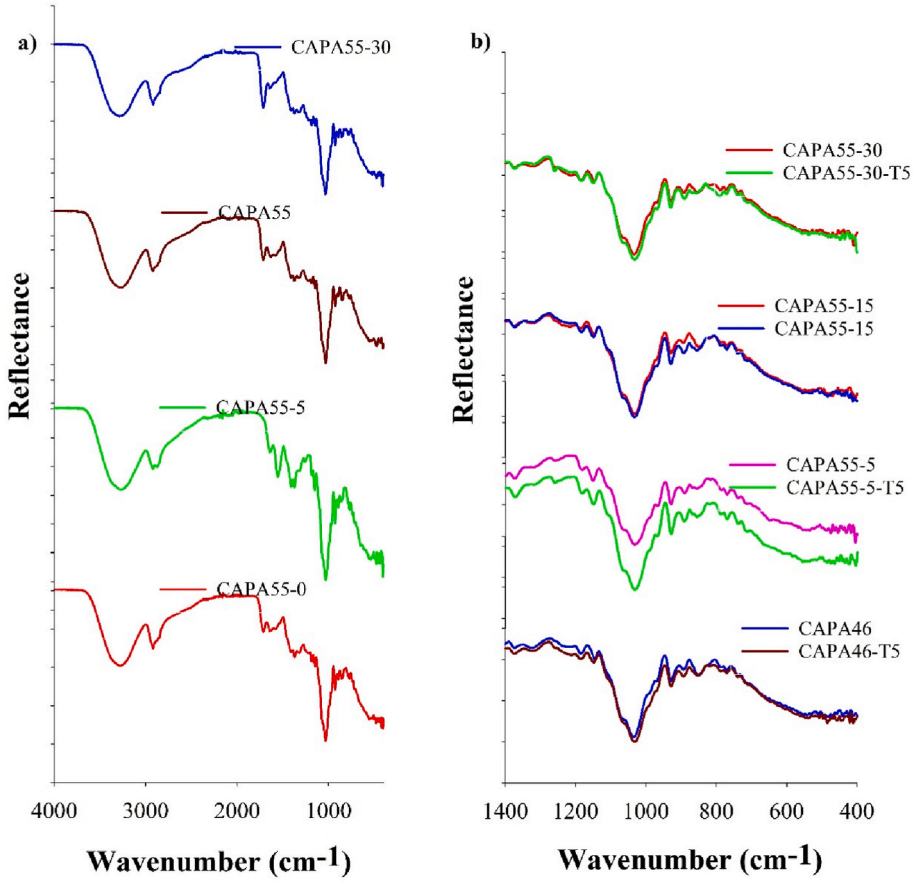

Fig. 5. a) FT-IR spectra of the agar/chitosan – agar/PVA bilayered composites films depending on the citric acid concentrations and **b)** comparison of the FT-IR spectra of the bilayered films in function of the drying temperatures at wavenumbers between 1400 and 400 cm^{-1}.

cases. The broad band at around 3330 cm^{-1} appearing for the pure agarose spectrum, shifted to 3260 cm^{-1} in the CAPA films. The most intense bands in agarose were detected at wavenumbers of about 1037, 967, 929, 890, 769, and 738 cm^{-1}. Therefore, as expected, the unlayered CAPA10 films with a predominance of agar in the formulation showed higher spectrum similarity with agarose in contrast to CAPA01.

Pure chitosan films (Fig. S3, as supplementary material) have been shown to exhibit a similar absorption at around 3329 cm^{-1} that was located between 3291 and 3261 cm^{-1} by Choo, Ching, Chuah, Julai, and Liou (2016). An analogous band was detected in the range of around 3279 cm^{-1} and found between 3301 cm^{-1} and 3257 cm^{-1} for PVA films (Ghorpade, Dias, Mali, & Mulla, 2019). This band appeared at around 3300 cm^{-1} for agar (Diop et al., 2022) and at around 3330 cm^{-1} for agarose (Fig. S3). The absorptions in this spectral range were mostly attributed to the *N*–H and *O*–H stretching vibrations. As the crosslinked PVA/agar layer in the bilayered films increased, the bands slightly shifted to lower wavenumbers, from 3267 cm^{-1} in the unlayered chitosan/agar blend film (CAPA10) to around 3258 cm^{-1} for the unlayered crosslinked PVA/agar blend (CAPA01). This shift could be related to absence of *N*–H stretching of the chitosan in this broad band. With the increase of the second layer, both band intensity and area were gradually lowered, which was particularly visible for CAPA64. Moreover, the CAPA01 and double layered films showed a typical band at around 2938 cm^{-1} assigned to the asymmetric *C*–H stretching mode, while the CAPA10 film displayed the same band at around 2921 cm^{-1}. This band generally appears at 2936 cm^{-1} for pure PVA. All tested films, except for CAPA10, showed additional bands at 1415 (1427 cm^{-1}), 1325 (1327 cm^{-1}) and 842 cm^{-1} (839 cm^{-1}) that could be attributed to the *C*–H bending of PVA (Nugroho, Nizardo, & Saepudin, 2020).

Authors such as Mali, Dhawale, Dias, Dhane, and Ghorpade (2018) evaluated the FT-IR spectra of pure citric acid and found prominent bands at 3279 cm^{-1} attributed to the ν(-OH) and at 1693 cm^{-1} attributed to the hydrogen ν(C=O). With the exception of CAPA10 deprived of citric acid, the band recorded at around 1713 cm^{-1} in the other films can be attributed to the ν(C=O) mode, localized in the bond resulting from the esterification of the PVA and agar polymers due to the presence of citric acid. Mali et al. (2018) also reported that the FT-IR bands appearing between 1710 and 1730 cm^{-1} cand be assigned to the carbonyl bond of free carboxylic acid groups and the carbonyl band of ester formed during crosslinking. This was in accordance with several studies, such as Nugroho et al. (2020), who corroborated the attribution of this peak at around 1713 cm^{-1} to the crosslinking effect of citric acid. Citric acid action is generally performed through ionic covalent crosslinking with the different polymers impacting, therefore, the chemical structure of the films (Czibulya et al., 2021). It was noticed that the unlayered crosslinked PVA/agar-based film had the highest band intensity at 1713 cm^{-1}. This observation could support the claim given for the double layered films that this peak's intensity increased as the second layer's volume increased in the film. As a result, it might be evidence of effective interactions between the different blended polymers on the one hand and between the two different layers on the other hand.

In contrast, the augmentation of the second layer's volume in the film, tended to progressively reduce the intensity of the absorptions appearing at around 1645 cm^{-1}, 1574 cm^{-1} and 1318 cm^{-1}. These bands were clearly perceptible for the CAPA10 film but not recorded for the CAPA01 film deprived of chitosan. Staroszczyk, Sztuka, Wolska, Wojtasz-Pająk, and Kołodziejska (2014) have assigned these peaks to respectively the amide I (νC=O) (amide carbonyl), amide II (δNH/νC=O) and amide III (νC-N and δC-*N*-H) molecules in chitosan in the presence of ester groups (Prabu & Natarajan, 2012). For these

authors, the amide I band related to a C=O vibration indicate the presence of acetyl (CH_3–C=O) groups in a chitosan molecule whilst Liu., Shen, Zhou, Wang & Deng (2016) located these bands at 1642, 1577 cm-1 and 1326 cm^{-1} for respectively amide I, II and III. Chitosan used in this study was over 75% deacetylated, therefore amide bands were not detected in pure chitosan spectrum. The appearing of the new bands related to the presence of amide could therefore corroborate a cross-linking of the chitosan in the first layer due to the citric acid presents in the second layer. Liu, Shen, Zhou, Wang, & Deng, 2016 reported similar situation and described the crosslinking happened through condensation polymerization between citric acid, amine and carboxyl. The intensities ratio I_{1037}/I_{1080} in CAPA films seems to increase with the percentage of chitosan-rich layer in the bilayered films. The bands detected at around 930, 872, and 770 cm-1 are specific to the 3, 6-anhydro-β-galactose skeletal bending characteristic of the agar biopolymer fraction (Diop et al., 2022). Fig. 5-a also depicts FT-IR spectra in relation to a double-layered film structure as a result of the citric acid concentration in the PVA/agar blend layer and the drying temperatures. With the increase of the crosslinking agent in the formulation of the films' second layer, it was evident that the band at 1713 cm-1, which is attributed to the C=O ester group, increased in intensity. This is observed for CAPA55 and CAPA55-30.

Fig. 5-b compares the variation of the FT-IR spectra of the double layered films at various crosslinking agent concentrations and drying temperatures at wavenumbers between 1400 and 400 cm^{-1}. Except for CAPA55-5 (5% citric acid) which showed a spectrum appearing at slightly higher reflectance at a lower drying temperature (45 °C), FT-IR does not reveal a noticeable impact of an increase in the drying temperature on the structural properties of the films containing citric acid.

3.4. Mechanical properties

Fig. 6(a–c) shows the stress-strain curves, Young's modulus (MPa), elongation at break (%), and tensile strength (MPa) of different bilayered composite films made by layering an PVA/agar formulation on top of an agar/chitosan blend. The visible elastic and plastic regions of the unlayered films (CAPA10 and CAPA01) showed differences in structural properties. Fig. 6-a illustrated a more brittle CAPA10 film, which was characterized by a sharp elastic region coupled with a short plastic region. The elastic zone represents the sharp straight line appearing at lower strain on the stress-strain curves. This zone was wider for the CAPA10, leading the film to break whenever the stress surpassed the elastic limit. Due to PVA's excellent film-forming capabilities, the narrower elastic region and wider plastic region observed for CAPA01 were indicative of a higher film's plasticity, also commonly observed for pure PVA film (Musetti et al., 2014). Therefore, using the PVA/agar blend to overlay a primary agar/chitosan layer had a visible effect on the mechanical properties of the resulting double-layered composite films. As a result, as the volume of the second layer increased, the films' capacity to return to their initial position (plasticity) decreased and the deformation increased. This phenomenon contributed to the validation of the two layers' complementing mechanical performances, fostered particularly by a good adhesion. Fig. 6-d clearly demonstrated the differences in Young's modulus of the different films. Similarly, the higher Young's modulus value for CAPA10 (Fig. 6-d) which expresses the ratio of

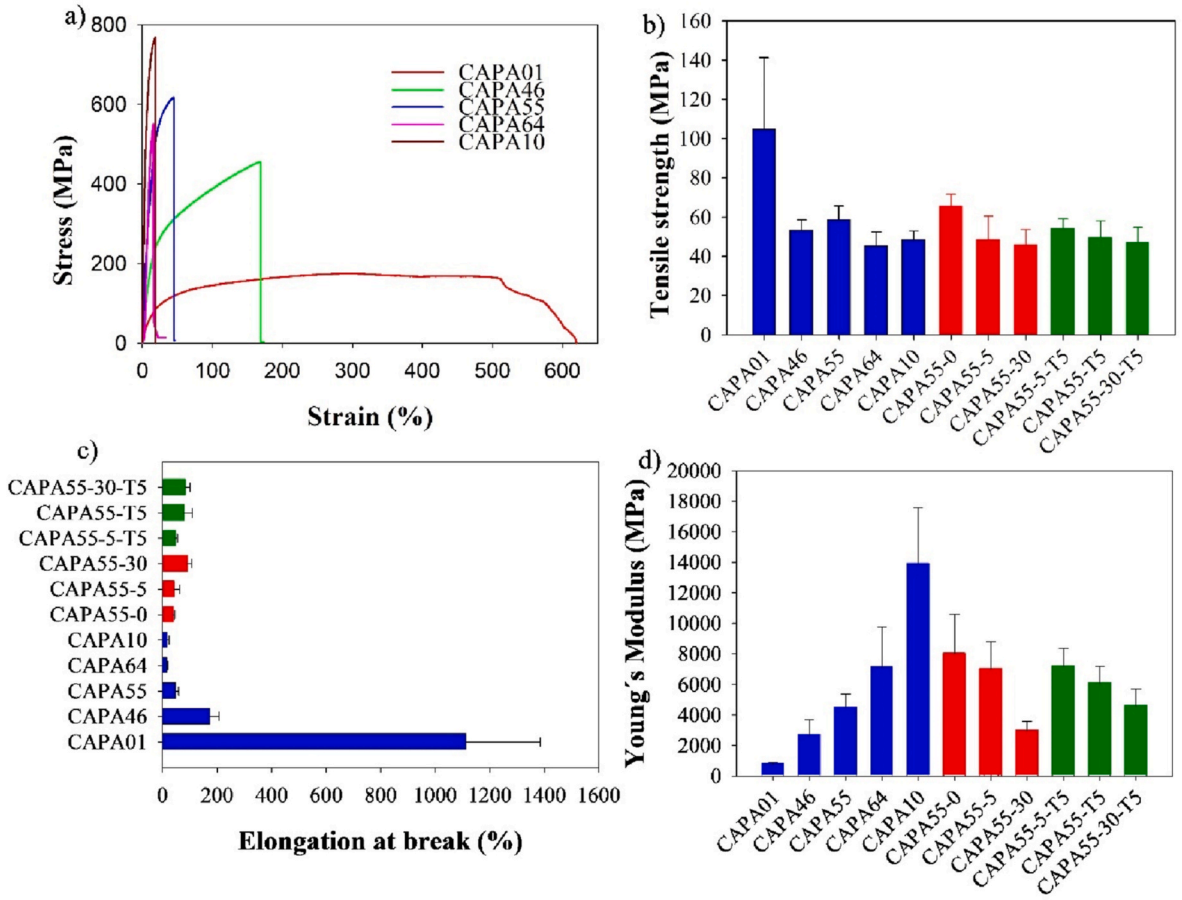

Fig. 6. Mechanical properties of the bilayered composite films. a) stress strain curve to the composite films in function of the layer volume variation. **b)** tensile strength of the bilayered composite films. **c)** variation of the elongation at break of the bilayered composite films **d)**. Young's modulus of the different bilayered composite films.

longitudinal stress to longitudinal strain, decreased as the volume of the PVA/agar layer increased ($p = 0.03$). The formed double-layered films, on the other hand, were more rigid in comparison to CAPA01, which was predominately affected by the presence of PVA over agar. Pearson moment correlation supported a strong negative but statistically significant relationship ($r = -095$, $p = 0.012$) between the volume fluctuation of the second layer and the Young's modulus. The citric acid used as a cross-linking agent in the PVA/agar formulation, on the other hand, tended to lower the Young's modulus. The Young's modulus values of the bilayered films were found to decrease gradually as citric acid content increased from 0 to 30% ($r = -092$, $p = 0.07$). However, increasing the drying temperature to 55 °C had only minor effects on the Young's modulus values, which were particularly noticeable at higher citric acid contents (15 and 30%).

Fig. 6-b depicts the effect of the composite film layer variation on tensile strength. Due to the predominance of the PVA polymer in CAPA01, the film displayed the highest tensile strength, as expected. However, the material's resistance to breaking was significantly reduced for the double-layered composite films. Despite the lack of statistical significance ($r = 0.823$, $p = 0.08$), it is worth mentioning that the tensile strength was found to be positively related to a subsequent variation of the volume of the second layers in the films. Some authors, such as Liu, Zhang, and Guo (2022) hypothesized that the increased tensile strength of PVA-based films was due to the higher content of –OH groups than polymers such as chitosan (Neto et al., 2005) or sulphated agar (Diop et al., 2022). As a result, the difference in tensile strength between the films could be explained by interfacial bonding between polymers within and between the layers. Given this, it is plausible that the interaction between PVA and agar in the second layer, and, more specifically, with the more acetylated chitosan in the first layer, altered the availability of hydroxyl groups, resulting in a lower strength. On the other hand, the large value difference between the fracture stress and the tensile strength noticed for the unlayered CAPA10 film (Fig. 6-a-b) can be the result of its high brittleness.

Crosslinking the PVA/agar (Fig. 6-b) appeared to be negatively correlated to the tensile strength of the bilayered composite films ($r = -0.408$, $p = 0.592$), as also observed for the Young's modulus. This trend persisted even if the drying temperature was raised to 55 °C. In contrast, the presence of citric acid in the formulation seemed to have a favorable impact on the elongation at break of the bilayered composites, as shown in Fig. 6 c, regardless of the drying temperature involved, as also observed by Shi et al. (2008). In terms of volume differences between the two different layers in the films, increasing the proportion of the crosslinked PVA/agar fraction in the composite material increased the ratio between the initial length and the changed length of the films after rupture. In the same trend, the Pearson moment correlation indicated a strong relationship between tensile strength and elongation at break. Likewise, although not statistically significant, there was a strong positive relationship between the crosslinking effect of citric acid and the films' elongation at break ($r = 0.921$, $p = 0.07$). This relationship was, however, inverted for the Young's modulus and tensile strength ($r = -0.923$, $p = 0.076$), regardless of the drying temperature.

3.5. Water uptake and thickness swelling

Fig. 7(a–b) illustrates the variation of the percent water uptake and thickness swelling of the different films as a function of the soaking times. Regardless of the type of film tested, the water uptake rate was more important during the first hours of immersion and then tended to plateau. However, at room temperature (25 ± 2 °C), each film exhibited distinct absorption and swelling behaviors. Higher hydrophobicity was observed in the unlayered CAPA10 film made from the chitosan/agar blend. After 24 h of immersion, the maximum water uptake was around 14 ± 3% and 175 ± 5% for CAPA 10 and CAPA01, respectively, with the latter being dominated by crosslinked PVA/agar. The water resistance of the bilayered composite films formed from these two formulations was differently impacted. Therefore, due to the formation of two distinctive interfaces in the bilayered composite films, the augmentation of the volume of the PVA/agar second layer fostered a greater hydrophilicity. The first layer of the film acted as a tempering agent, which reduced the water absorption potential of the bilayered films as compared to CAPA01. The thickness swelling of the unlayered, and double layered films followed a similar trend and depended on the layers' volumes (Fig. 7-b).

Each biopolymer in the formulation tended to attract water molecules via hydrogen bonding, depending on its specific sensitivity to water. This phenomenon provokes reversible or irreversible swelling, which explains the weight variation as well as the thickness and/or linear expansion of the bilayered fraction (Abdulkhani, Marvast, Ashori, Hamzeh, & Karimi, 2013; Le Gars et al., 2020). The differences in sensitivity are mostly related to the modifications in the chemical structures of the macromolecules involved, particularly chitosan and PVA. PVA polymer makes it highly hydrophilic due to the abundance of free hydroxyl groups. Chitosan, on the other hand, is a water-insoluble polymer containing both acetyl and amine groups that increase its resistance (Gatto, Ochi, Yoshida, & da Silva, 2019). El-Hefian, Nasef, and Yahaya (2010) also reported an increase in water uptake in chitosan/PVA blend films as the PVA content increased.

It is important to note that agar, specially its agarose fraction, is water sensitive. The presence of sulfate units, on the other hand, tends to

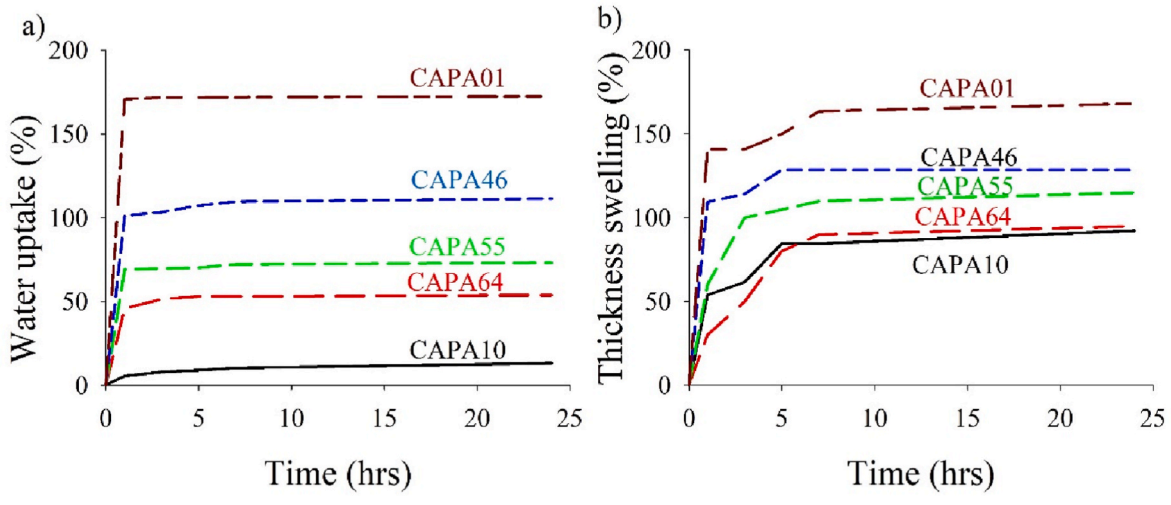

Fig. 7. Water absorption (a) and thickness swelling (b) of the bilayered composite films in function of the soaking time (hrs).

reduce the free hydroxyl groups on the molecule, making it more hydrophobic as compared to PVA. On the other hand, authors such as Awadhiya, Kumar, and Verma (2016) reported that the crosslinking effect of citric acid reduced the water uptake of pure agarose by up to 8.7 times. According to these authors, the interaction with citric acid resulted in a drastic decrease in the percent swelling due to a significant reduction in the freedom of movement of agarose chains in the film. The crosslinking effect of citric acid could function similarly with the free hydroxyl group of the deacetylated chitosan as observed for PVA principally at the interface of the two distinct layers.

3.6. X-ray diffraction analysis

The crystalline structure of the unlayered and bilayered films has been evaluated from the XRD patterns (Fig. 8 a-e). The unlayered agar/chitosan blend film (CAPA10) was distinguished by a small peak recorded at 2θ ≈ 13°, a prominent peak that appeared at around 2θ ≈ 20° and a minor broad shoulder at 2θ ≈ 40° (Fig. 8-a). Pure agar biopolymer films generally exhibit diffractograms characterized by a minor peak shoulder at 2θ ≈ 13.8° and a peak at 2θ ≈ 19.0°, indicating an orderly structure and semi-crystalline nature of the polymer matrix (Arfat, Ahmed, & Jacob, 2017). Guo, Zhang, Zhao, Qiao, and Xie (2021) have identified a broad peak at 2θ ≈ 19 for native agar, which is associated with its strong amorphous structure. Intermolecular hydrogen bonds in agar can form a double-helical conformation, which may confer lower crystallinity. Pure chitosan films, on the other hand, frequently exhibit distinct peaks at approximately 2θ ≈ 15° and 20°, which can be attributed to the reflection planes of (110) and (220) (Aziz, Abdulwahid, Rasheed, Abdullah, & Ahmed, 2017). The peak at around 2θ ≈ 20°, generally resulted from the contribution of two peaks at 2θ ≈ 20.16 and 2θ ≈ 21.80°, related to the reflections of (200) and (220) planes of hydrated chitosan polymorph (Osorio-Madrazo et al., 2010). These corresponding crystalline peaks ((110) and (220)) can indicate the average intermolecular distance of the crystalline parts of chitosan due to

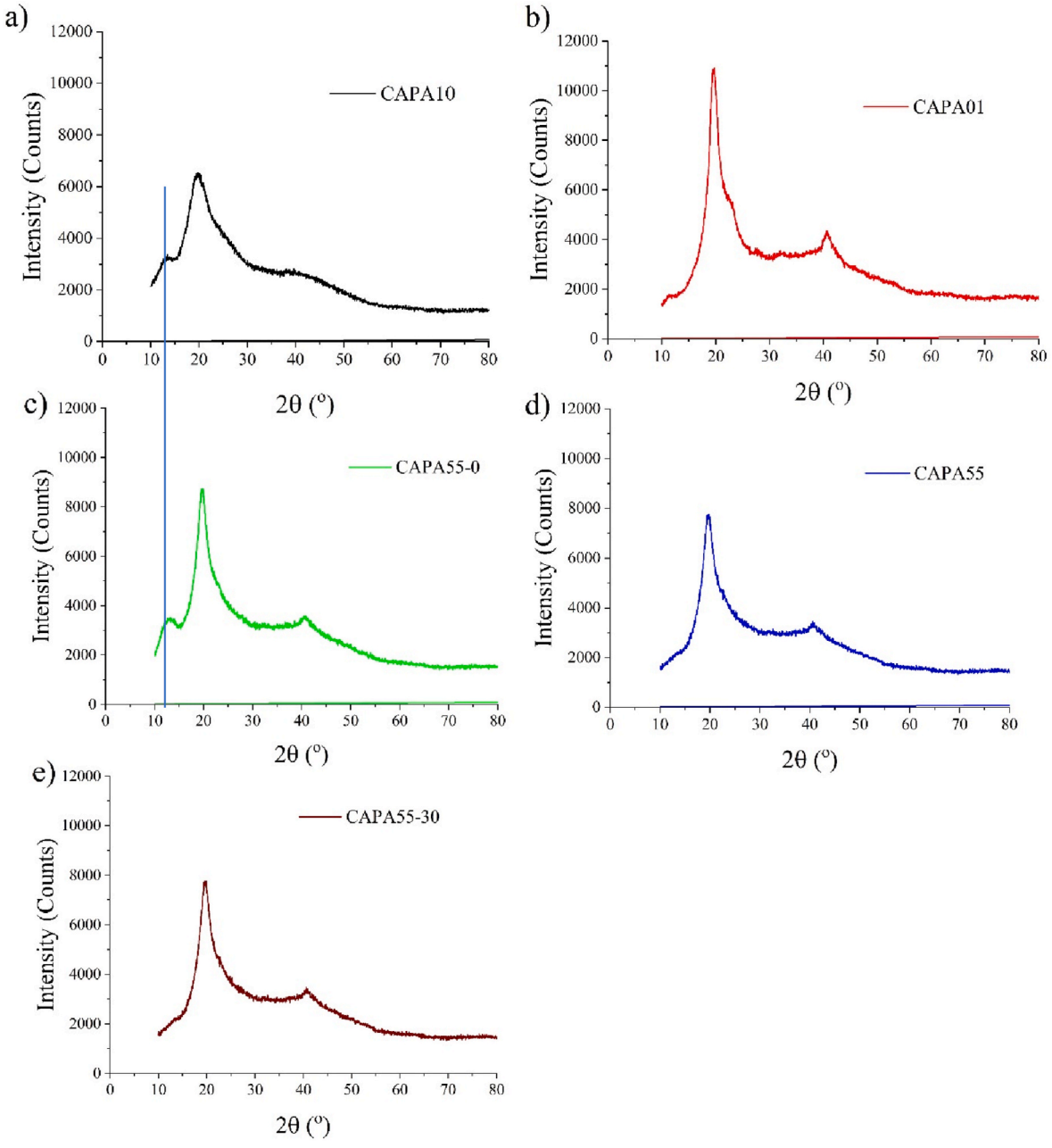

Fig. 8. (a–e) XRD spectra of the agar/chitosan – agar/PVA bilayered composite films.

intramolecular and intermolecular hydrogen bonds. An additional broad shoulder at 2θ ≈ 40° was assigned to the amorphous region of chitosan (Aziz et al., 2017). The XRD results demonstrated, therefore, that the crystalline structure of chitosan dominated the diffractogram in the CAPA10 (Fi. 7-a) film. Fig. 8-b shows the diffractogram of the unlayered CAPA01 film (PVA/agar/citric acid blend). CAPA01 displayed the typical crystallinity pattern of polyvinyl alcohol, characterized by sharp peaks at around 2θ = 20 and 40°. These peaks, which correspond to the crystalline domain and semicrystalline nature of pure PVA, supported intramolecular and intermolecular hydrogen bonding (Aziz, Kadir, Hamsan, Woo, & Brza, 2019). The strong peak at around 2θ = 20° is attributed to the (101) plane of the crystalline part of the semi-crystalline PVA polymer. According to authors such as Aziz et al. (2019), it denotes a high quantity of the crystalline domain in pure PVA.

The crystallinity of the CAPA01 film was dominated by the semi-crystalline structure of PVA over the amorphous structure of agar. The appearance of a new characteristic peak of the CAPA01 diffractogram did not indicate the presence of citric acid with small molecular and strong crystal diffractions.

On the other hand, modified diffractograms were obtained following the juxtaposition of the previously cited formulations to produce the bilayered composite films. As shown in Fig. 8-c, with the absence of natural organic acid as a crosslinking agent, the characteristic peaks observed in CAPA10 and CAPA01 (2θ ≈ 13, 20 and 40°) were also recorded in the bilayered films. This may indicate a good relationship between the distinct layers. However, the intensity of the sharp peak at 2θ ≈ 20° and 40° that was high for CAPA01 decreased substantially in the bilayered films. The presence of the first agar/chitosan blend layer influenced the crystallite structure of PVA, which dominated in CAPA01. It primarily denoted hydrogen bond interactions between PVA and chitosan. The crosslinking reaction due to citric acid contributed to the decrease of this peak. In a similar process, Jiang et al. (2020) have reported that the presence of citric acid could not significantly change the crystal structure of crosslinked konjac glucomannan/surface deacetylated chitin nanofibers. However, results, has shown that the higher the citric acid content, the lower the intensity (Fig. 8-c-d-e), of the peak at 2θ ≈ 13° (characteristic of chitosan). The strong decrease in this peak's intensity was considerable, and it tended to disappear at high citric acid contents in the bilayered films. Similar phenomena have also been reported by Wu et al. (2019) for citric acid crosslinked starch/chitosan composite films, where the crystallinity of starch film and chitosan film decreased with the crosslinking reaction of citric acid. The explanation proposed by Wen et al. (2021) for the carboxymethyl chitosan/PVA crosslinked network could be valid in the present study for the bilayered films. These authors related the lowering of these peaks to the interaction of the -COO^- of citric acid with –NH_3^+ of chitosan to form an ionic bond, which weakens the hydrogen bond between the PVA formulation and the chitosan formulation in the double layers. As also indicated by Jiang et al. (2020), the incorporation of citric acid into a polysaccharide system in the presence of chitin derivatives such as chitosan led to a lower crystallinity of the system.

3.7. Thermogravimetric analysis (TGA)

The TGA curves and derivative thermogravimetry profiles of the unlayered and bilayered composite films were shown in Fig. 9(a–b). Different stages of weight loss were observed for all tested films after being exposed to high temperatures (Fig. 9-a). The initial material weight was seen to be slightly reduced between 25 and 200 °C, whereas a more intense loss was noticed for CAPA10. The evaporation of the bound water in the films is typically responsible for the weight loss recorded in this temperature range. The reduction in evaporation at these temperatures is attributed by authors such as Martínez-Camacho et al. (2010) to a robust connection between the water molecules in the film and the glycerol used as the plasticizer. The successive weight losses noticed at higher temperature ranges were a result of the distinctive polymers in the bilayered composite films going through various stages of breakdown. The critical degradation stage of the unlayered CAPA10 composed of chitosan and agar is materialized by a broad peak between 160 and 340 °C in the derivative weight loss (DTG) profile (Fig. 9-b). The wide area of this peak might be related to the cumulative degradation phase of agar and chitosan at these temperatures. All films, including the unlayered CAPA01, which showed higher intensity than its bilayered counterparts, showed similar peaks. These latter films, however, showed significant degradation that occurred in two distinct phases, as evidenced by the DTG spectra (Fig. 9-b, peaks 2 and 3). For CAPA01, the initial stage might be connected to the progressive breakdown of the primary PVA chain and agar. The overall weight loss profile of the major PVA chain may be specifically allocated to the second degradation stage, which appears at temperatures between 300 and 400 °C (Shahi, Joshi, & Min, 2020).

It is important to notice that for CAPA01, the primary degradation in the second stage (Fig. 9-b, peak 2) took place at about 255 °C. For the bilayered films, such as CAPA55-0 (250 °C), CAPA55-30 (243 °C), and CAPA55 (247 °C), it appeared at slightly lower temperatures, indicating reduced film stability. This result could corroborate the hypothesis of a relationship between the film's formulation and its stability. In the same trend, the reduced PVA degradation intensity in this temperature range may be attributed to the double-layered structure, as is particularly evident for CAPA55-0 without citric acid. As the citric acid level increased from 0 to 30%, the crosslinking effect tended to reduce the material degradation. Fig. 9-b (peak 3) showed that the maximum

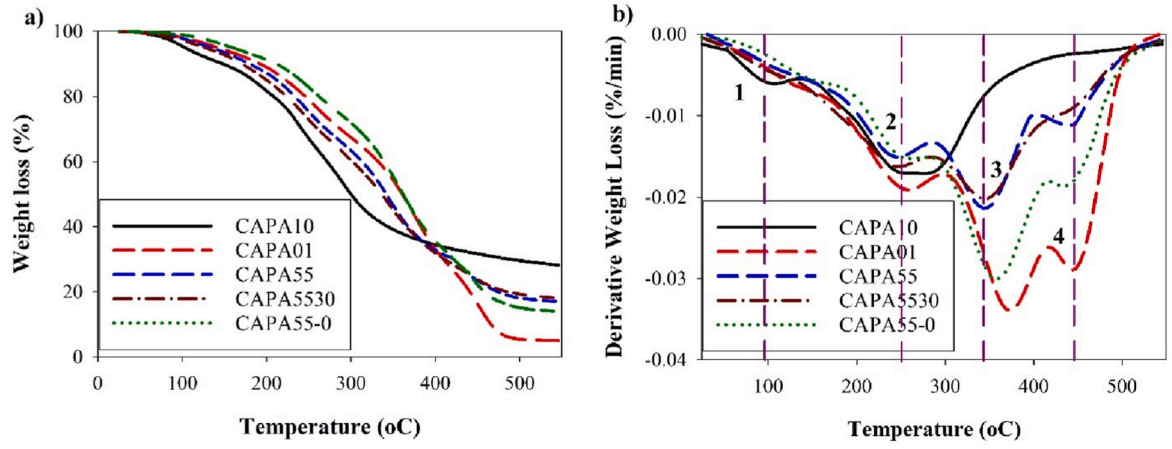

Fig. 9. Thermal stability of the agar/chitosan – agar/PVA bilayered composite films. **a)** weight loss variation and **b)** derivative weight loss.

degradation in the second phase occurred at around 374 °C for CAPA01. This maximum polymeric breakdown was recorded at a lower temperature of 358 °C for the double layered film CAPA55-0 deprived of citric acid. Increasing the concentration of the crosslinking agent, therefore, resulted in the lowering of the polymeric degradation temperature to approximately 355 °C for CAPA55 (15% citric acid) and 343 °C for CAPA55-30 (30% citric acid), respectively. The third degradation phase of the main PVA chain displayed in Fig. 9-b (peak 4) was visible in the temperature range of 400–500 °C with a maximum degradation at about 445 °C for all films containing PVA. However, citric acid's beneficial effects on the stability of composite films are generally confirmed by the decrease in peak intensity (peaks 3 and 4) that happened when the crosslinking agent concentration in the composite films increased. Additionally, CAPA01 film, which exhibited a lower char residue (5.22 ± 0.5%), likewise degraded more quickly. The bilayered film structure therefore helped reduce the carbonaceous residues at 550 °C under nitrogen in contrast to the unlayered CAPA10 (28.03 ± 0.3% char) film. However, as compared to the unlayered CAPA01, the increase in citric acid in films tended to increase the amount of residual char (CAPA55-0 = 13.75 ± 0.5, CAPA55-15 = 17.73 ± 0.2, and CAPA55.30 = 17.74 ± 0.4). Citric acid, according to Yurong and Dapeng (2020), significantly increased the thermal stability of a starch/PVA composite film by interacting with the chains of both starch and PVA.

3.8. Microstructure of the composite films

The composite films exhibited smooth, uniform surfaces, free of cracks and visible pores. This microstructure could confirm good polymer adhesion, particularly between the agar present in both formulations, and respectively, the water insoluble chitosan and PVA polymer in the distinctive films.

The individual biopolymers seemed to form a continuous, homogeneous aspect, as seen in the cross section of the films. Furthermore, the bilayer films, were characterized by homogenous and dense layer structures having strong interfacial adhesion. Fig. 10(a–d) depicts the fractured composite films' cross-sectional morphology. Good interlayer adhesion is a critical parameter for avoiding delamination, which could affect the mechanical and barrier properties of the films (Slavutsky, Gamboni, & Bertuzzi, 2018). Micrographs showed tightly bound structure between the two layers due to good surface interaction (Fig. 10-*c*-d), as compared to the unlayered films (Fig. 10-a-b). As a result of the interacting reinforcement effect fostered by the presence of agar in both layer formulations, the phase separation appeared unclear in all double-layered films. This could denote a sign of high compatibility and homogeneity at the interface between the agar/chitosan and the crosslinked PVA/agar layers (Romruen, Kaewprachu, Karbowiak, & Rawdkuen, 2022). PVA being rich in hydroxyl groups (Le Gars et al., 2020), the second layer seems to be integrated with the first agar/chitosan rich layer.

Similarly, Chen et al. (2019) demonstrated that the presence of residual moisture on the first starch layer contributed to extending the evaporation time during the preparation of a starch/Zein bilayer film. Therefore, it was stated that this phenomenon enabled the zein layer to move freely and fully integrate into the starch layer. This assertion implies that casting the second layer on top of the never-dried gel-like structure of the agar/chitosan will considerably reinforce the interfacial imbrication of the two layers upon drying. A homogeneous dispersion of the second layer may improve chemical affinity at the interface, resulting in increased mechanical strength. The impact of citric acid on the microstructure of the films has been evaluated. Results seemed to

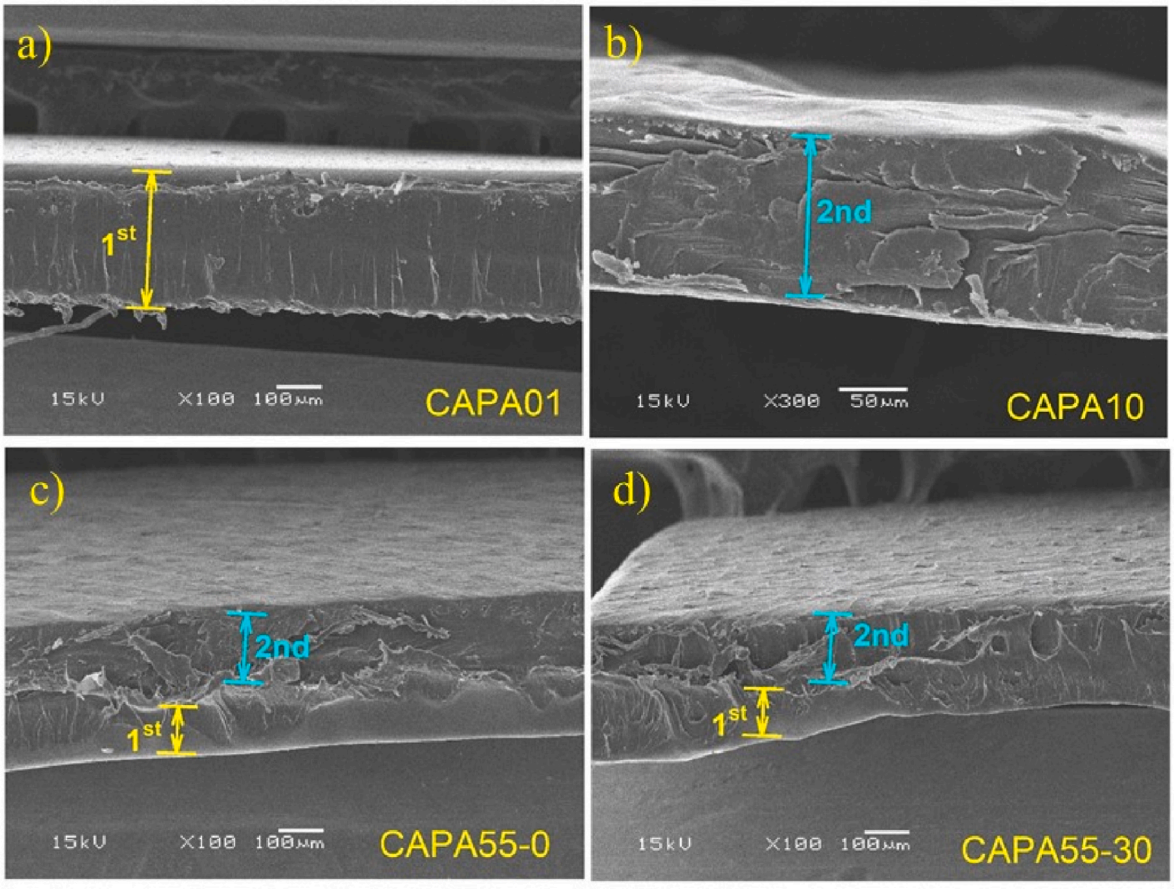

Fig. 10. Microstructure of the cross-section of a) the unilayered agar/PVA films (CAPA01), b) the unlayered agar/chitosan film (CAPA10), c) the double layered composite films at a 50:50 vol ratio at 0% citric acid, and d) the double layered composite films at a 50:50 vol ratio at 30% citric acid.

indicate that the presence of crosslinking agent fostered a better homogeneity between the two layers. It results in less perceptible demarcation between layers for CAPA55-30 with 30% citric acid (Fig. 10-d) as compared to CAPA55-0 without crosslinking agent (Fig. 10-c). Nonetheless, the overall impact of citric acid on the microscopic structure of the film as observed through SEM was relatively restrained.

4. Conclusion

A layer-by-layer casting method has been proposed as a technological process for producing strong double layer biobased plastic. The physico-mechanical properties of the double-layered films were clearly influenced by changes in the volumes of the agar/chitosan and PVA/agar layers. The use of glycerol improved the plasticity and foldability of the films, while citric acid at various concentrations acted as a crosslinking agent in the PVA/agar formulation. During the film processing conditions, effective molecular interactions were evidenced by the change in the FT-IR spectra observed for the bilayer films as compared to the unlayered controls. The exploitation of the good-forming ability of PVA with abundant hydroxyl groups and the presence of agar fostered adhesion between the layers. The mechanical properties of the films were principally dependent on the volume of the second layer in relation to the total film's volume. It suggested that the layer-by-layer casting fabrication of these bilayer films from a first layer of never-dried agar/chitosan was an alternative solution for multi-layered fossil-based plastic replacement. The crosslinking effect of citric acid had a major impact on the change of the semi-crystalline structure of the bilayer composites, which was initially dominated by the chitosan and PVA structures. The films displayed semi-transparency and UV-light blocking properties that were beneficial in preventing phenomena such as lipid oxidation. The increased hydrophobicity of the bilayer films could increase their potential use in a wide range of applications for the packaging of dry and low moisture food products.

Declaration of competing interest

The authors declare that they have no known competing financial interests or personal relationships that could have appeared to influence the work reported in this paper

Data availability

No data was used for the research described in the article.

Acknowledgement

This work was supported by the European Commission, Horizon 2020 program through the Marie-Curie Individual Fellowship (H2020-MSCA-IF-2019), with regards to the ALGWAS-BIOR project (Grant agreement number 898804). This work was also supported by European Union H2020-LC-SC3-2020-NZE-RES-CC, NMBP-16-2020-GA 953152 and DT-NMBP-04-2020 Projects and Ministerio deand Ministerio de Ciencia, Innovación y Universidades CTQ(QMC) RED 2018-102471-T MultiMetDrugs Network (Spain).

Appendix A. Supplementary data

Supplementary data to this article can be found online at https://doi.org/10.1016/j.foodhyd.2023.108987.

References

Abdulkhani, A., Marvast, E. H., Ashori, A., Hamzeh, Y., & Karimi, A. N. (2013). Preparation of cellulose/polyvinyl alcohol biocomposite films using 1-n-butyl-3-methylimidazolium chloride. *International Journal of Biological Macromolecules, 62*, 379–386. https://doi.org/10.1016/j.ijbiomac.2013.08.050

Agusman Fransiska, D., Murdinah Wahyuni, T., Irianto, H. E., Priambudi, P., Fateha Abdullah, A. H. D., Nissa, R. D., et al. (2022). Physical properties of bioplastic agar/chitosan blend. *IOP Conference Series: Earth and Environmental Science, 978*(1). https://doi.org/10.1088/1755-1315/978/1/012046

Andreeßen, C., & Steinbüchel, A. (2019). Recent developments in non-biodegradable biopolymers: Precursors, production processes, and future perspectives. *Applied Microbiology and Biotechnology, 103*(1), 143–157. https://doi.org/10.1007/s00253-018-9483-6

Arfat, Y. A., Ahmed, J., & Jacob, H. (2017). Preparation and characterization of agar-based nanocomposite films reinforced with bimetallic (Ag-Cu) alloy nanoparticles. *Carbohydrate Polymers, 155*, 382–390. https://doi.org/10.1016/j.carbpol.2016.08.097

Awadhiya, A., Kumar, D., & Verma, V. (2016). Crosslinking of agarose bioplastic using citric acid. *Carbohydrate Polymers, 151*, 60–67. https://doi.org/10.1016/j.carbpol.2016.05.040

Aziz, S., Abdulwahid, R., Rasheed, M., Abdullah, O., & Ahmed, H. (2017). Polymer blending as a novel approach for tuning the SPR peaks of silver nanoparticles. *Polymers, 9*(12), 486. https://doi.org/10.3390/polym9100486

Aziz, S. B., Kadir, M. F. Z., Hamsan, M. H., Woo, H. J., & Brza, M. A. (2019). Development of polymer blends based on PVA:POZ with low dielectric constant for microelectronic applications. *Scientific Reports, 9*(1), Article 13163. https://doi.org/10.1038/s41598-019-49715-8

Basumatary, I. B., Mukherjee, A., Katiyar, V., & Kumar, S. (2022). Biopolymer-based nanocomposite films and coatings: Recent advances in shelf-life improvement of fruits and vegetables. *Critical Reviews in Food Science and Nutrition, 62*(7), 1912–1935.

Brennan, L., Langley, S., Verghese, K., Lockrey, S., Ryder, M., Francis, C., et al. (2021). The role of packaging in fighting food waste: A systematised review of consumer perceptions of packaging. *Journal of Cleaner Production, 281*. https://doi.org/10.1016/j.jclepro.2020.125276

Cazón, P., Vázquez, M., & Velazquez, G. (2019). Composite films with UV-barrier properties based on bacterial cellulose combined with chitosan and poly(vinyl alcohol): Study of puncture and water interaction properties. *Biomacromolecules, 20*(5), 2084–2095. https://doi.org/10.1021/acs.biomac.9b00317

Chen, X., Cui, F., Zi, H., Zhou, Y., Liu, H., & Xiao, J. (2019). Development and characterization of a hydroxypropyl starch/zein bilayer edible film. *International Journal of Biological Macromolecules, 141*, 1175–1182. https://doi.org/10.1016/j.ijbiomac.2019.08.240

Choo, K., Ching, Y., Chuah, C., Julai, S., & Liou, N.-S. (2016). Preparation and characterization of polyvinyl alcohol-chitosan composite films reinforced with cellulose nanofiber. *Materials, 9*(8), 644. https://doi.org/10.3390/ma9080644

Czibulya, Z., Csík, A., Tóth, F., Pál, P., Csarnovics, I., Zelkó, R., et al. (2021). The effect of the PVA/chitosan/citric acid ratio on the hydrophilicity of electrospun nanofiber meshes. *Polymers, 13*(20), 3557.

Diop, C. I. K., Lavoie, J.-M., & Huneault, M. A. (2017). Separation and reuse of multilayer food packaging in cellulose reinforced polyethylene composites. *Waste and Biomass Valorization, 8*(1), 85–93. https://doi.org/10.1007/s12649-016-9605-2

Diop, C. I. K., Li, H. L., Xie, B. J., & Shi, J. (2011). Effects of acetic acid/acetic anhydride ratios on the properties of corn starch acetates. *Food Chemistry, 126*(4), 1662–1669. https://doi.org/10.1016/j.foodchem.2010.12.050

Diop, C. I. K., Trigueros, E., Sanz, M. T., Beltran, S., & García-Tojal, J. (2022). Pressurized hot water-assisted recovery of crude residual agar from a never-dried algae industry waste stream: A box-behnken design approach. *Food Hydrocolloids, 129*(February), Article 107664. https://doi.org/10.1016/j.foodhyd.2022.107664

El-Hefian, E. A., Nasef, M. M., & Yahaya, A. H. (2010). The preparation and characterization of chitosan/poly (vinyl alcohol) blended films. *E-Journal of Chemistry, 7*(4), 1212–1219. https://doi.org/10.1155/2010/626235

European Commission. (2022). *On packaging and packaging waste*. amending Regulation (EU), 5. 2019/1020 and Directive (EU) 2019/904, and repealing Directive 94/62/EC https://eur-lex.europa.eu/legal-content/EN/ALL/?uri=COM:2022:677:FIN.

Food and Agriculture Organization of the United Nations. (2009). *The state of food and agriculture. moving forward on food loss and waste reduction*.

Gatto, M., Ochi, D., Yoshida, C. M. P., & da Silva, C. F. (2019). Study of chitosan with different degrees of acetylation as cardboard paper coating. *Carbohydrate Polymers, 210*, 56–63. https://doi.org/10.1016/j.carbpol.2019.01.053

Ghorpade, V. S., Dias, R. J., Mali, K. K., & Mulla, S. I. (2019). Citric acid crosslinked carboxymethylcellulose-polyvinyl alcohol hydrogel films for extended release of water soluble basic drugs. *Journal of Drug Delivery Science and Technology, 52*, 421–430. https://doi.org/10.1016/j.jddst.2019.05.013

Greenpeace. (2022). *New Greenpeace report: Plastic recycling is a dead-end street—Year after year, plastic recycling declines even as plastic waste increases*. Available online: https://www.greenpeace.org/usa/news/new-greenpeace-report-plastic-recycling-is-a-863dead-end-street-year-after-year-plastic-recycling-declines-even-as-plastic-waste-864increases/. Available online: (last accessed June 29 2023).

Guo, Y., Zhang, B., Zhao, S., Qiao, D., & Xie, F. (2021). Plasticized starch/agar composite films: Processing, morphology, structure, mechanical properties and surface hydrophilicity. *Coatings, 11*(3), 311. https://doi.org/10.3390/coatings11030311

Haghighi, H., Gullo, M., La China, S., Pfeifer, F., Siesler, H. W., Licciardello, F., et al. (2021). Characterization of bio-nanocomposite films based on gelatin/polyvinyl alcohol blend reinforced with bacterial cellulose nanowhiskers for food packaging applications. *Food Hydrocolloids, 113*. https://doi.org/10.1016/j.foodhyd.2020.106454

Hosseini, S. F., Javidi, Z., & Rezaei, M. (2016). Efficient gas barrier properties of multilayer films based on poly(lactic acid) and fish gelatin. *International Journal of Biological Macromolecules, 92*, 1205–1214. https://doi.org/10.1016/j.ijbiomac.2016.08.034

Infurna, G., Cavallaro, G., Lazzara, G., Milioto, S., & Dintcheva, N. T. (2022). Effect of different processing techniques and presence of antioxidant on the chitosan film performance. *Journal of Vinyl and Additive Technology, 28*(2), 343–351. https://doi.org/10.1002/vnl.21905

Jiang, H., Sun, J., Li, Y., Ma, J., Lu, Y., Pang, J., et al. (2020). Preparation and characterization of citric acid crosslinked konjac glucomannan/surface deacetylated chitin nanofibers bionanocomposite film. *International Journal of Biological Macromolecules, 164*, 2612–2621. https://doi.org/10.1016/j.ijbiomac.2020.08.138

Jose, J., & Al-Harthi, M. A. (2017). Citric acid crosslinking of poly(vinyl alcohol)/starch/graphene nanocomposites for superior properties. *Iranian Polymer Journal (English Edition), 26*(8), 579–587. https://doi.org/10.1007/s13726-017-0542-0

Le Gars, M., Dhuiège, B., Delvart, A., Belgacem, M. N., Missoum, K., & Bras, J. (2020). High-barrier and antioxidant poly(lactic acid)/nanocellulose multilayered materials for packaging. *ACS Omega, 5*(36), 22816–22826. https://doi.org/10.1021/acsomega.0c01955

Lee, B. X., Kjaerulf, F., Turner, S., Cohen, L., Donnelly, P. D., Muggah, R., et al. (2016). Transforming our world: Implementing the 2030 agenda through sustainable development goal indicators. *Journal of Public Health Policy, 37*(1), S13–S31. https://doi.org/10.1057/s41271-016-0002-7

Lipatova, I. M., & Yusova, A. A. (2021). Effect of mechanical activation on starch crosslinking with citric acid. *International Journal of Biological Macromolecules, 185*, 688–695.

Liu, Y., Shen, X., Zhou, H., Wang, Y., & Deng, L. (2016). Chemical modification of chitosan film via surface grafting of citric acid molecular to promote the biomineralization. *Applied Surface Science, 370*, 270–278.

Liu, B., Zhang, J., & Guo, H. (2022). Research progress of polyvinyl alcohol water-resistant film materials. *Membranes, 12*(3). https://doi.org/10.3390/membranes12030347

Mali, K. K., Dhawale, S. C., Dias, R. J., Dhane, N. S., & Ghorpade, V. S. (2018). Citric acid crosslinked carboxymethyl cellulose-based composite hydrogel films for drug delivery. *Indian Journal of Pharmaceutical Sciences, 80*(4), 657–667.

Martínez-Camacho, A. P., Cortez-Rocha, M. O., Ezquerra-Brauer, J. M., Graciano-Verdugo, A. Z., Rodriguez-Félix, F., Castillo-Ortega, M. M., et al. (2010). Chitosan composite films: Thermal, structural, mechanical and antifungal properties. *Carbohydrate Polymers, 82*(2), 305–315. https://doi.org/10.1016/j.carbpol.2010.04.069

Mohanty, F., & Swain, S. K. (2017). Bionanocomposites for food packaging applications. In *Nanotechnology applications in food: Flavor, stability, nutrition and safety* (pp. 363–379). Elsevier Inc. https://doi.org/10.1016/B978-0-12-811942-6.00018-2.

Mujtaba, M., Morsi, R. E., Kerch, G., Elsabee, M. Z., Kaya, M., Labidi, J., et al. (2019). Current advancements in chitosan-based film production for food technology; A review. *International Journal of Biological Macromolecules, 121*, 889–904. https://doi.org/10.1016/j.ijbiomac.2018.10.109

Musetti, A., Paderni, K., Fabbri, P., Pulvirenti, A., Al-Moghazy, M., & Fava, P. (2014). Poly(vinyl alcohol)-based film potentially suitable for antimicrobial packaging applications: PVOH film for active packaging. *Journal of Food Science, 79*(4), E577–E582. https://doi.org/10.1111/1750-3841.12375

Neto, C. G. T., Giacometti, J. A., Job, A. E., Ferreira, F. C., Fonseca, J. L. C., & Pereira, M. R. (2005). Thermal analysis of chitosan based networks. *Carbohydrate Polymers, 62*(2), 97–103. https://doi.org/10.1016/j.carbpol.2005.02.022

Nugroho, F. G., Nizardo, N. M., & Saepudin, E. (2020). *Synthesis of citric acid crosslinked PVA/tapioca starch bioplastic reinforced with grafted cellulose*, Article 040040. https://doi.org/10.1063/5.0010357

OECD. (2022). *Global plastics outlook: Economic drivers, environmental impacts and policy options*.

Ojogbo, E., Ogunsona, E. O., & Mekonnen, T. H. (2020). Chemical and physical modifications of starch for renewable polymeric materials. *Materials Today Sustainability, 7*(8), Article 100028. https://doi.org/10.1016/j.mtsust.2019.100028

Osorio-Madrazo, A., David, L., Trombotto, S., Lucas, J.-M., Peniche-Covas, C., & Domard, A. (2010). Kinetics study of the solid-state acid hydrolysis of chitosan: Evolution of the crystallinity and macromolecular structure. *Biomacromolecules, 11*(5), 1376–1386. https://doi.org/10.1021/bm1001685

Park, K., Oh, Y., Panda, P. K., & Seo, J. (2022). Effects of an acidic catalyst on the barrier and water resistance properties of crosslinked poly (vinyl alcohol) and boric acid films. *Progress in Organic Coatings, 173*, Article 107186.

Prabu, K., & Natarajan, E. J. A. A. S. (2012). Isolation and FTIR spectroscopy characterization of chitin from local sources. *Advances in Applied Science Research, 3*(2), 1870–1875.

Rahman, M. H., & Bhoi, P. R. (2021). An overview of non-biodegradable bioplastics. *Journal of Cleaner Production, 294*. https://doi.org/10.1016/j.jclepro.2021.126218

Romruen, O., Kaewprachu, P., Karbowiak, T., & Rawdkuen, S. (2022). Development of smart bilayer alginate/agar film containing anthocyanin and catechin-lysozyme. *Polymers, 14*(22), 5042. https://doi.org/10.3390/polym14225042

Shahi, N., Joshi, G., & Min, B. (2020). Effect of regenerated cellulose fibers derived from black oat on functional properties of PVA-based biocomposite film. *Processes, 8*(9), 1149. https://doi.org/10.3390/pr8091149

Shi, R., Bi, J., Zhang, Z., Zhu, A., Chen, D., Zhou, X., et al. (2008). The effect of citric acid on the structural properties and cytotoxicity of the polyvinyl alcohol/starch films when molding at high temperature. *Carbohydrate Polymers, 74*(4), 763–770. https://doi.org/10.1016/j.carbpol.2008.04.045

Slavutsky, A. M., Gamboni, J. E., & Bertuzzi, M. A. (2018). Formulation and characterization of bilayer films based on Brea gum and Pectin. *Brazilian Journal of Food Technology, 21*(0). https://doi.org/10.1590/1981-6723.21317

Sonneveld, K., James, K., Fitzpatrick, L., & Lewis, H. (2005). Sustainable packaging: How do we define and measure it. In *In 22nd IAPRI symposium* (pp. 1–9).

Staroszczyk, H., Sztuka, K., Wolska, J., Wojtasz-Pająk, A., & Kołodziejska, I. (2014). Interactions of fish gelatin and chitosan in uncrosslinked and crosslinked with EDC films: FT-IR study. *Spectrochimica Acta Part A: Molecular and Biomolecular Spectroscopy, 117*, 707–712. https://doi.org/10.1016/j.saa.2013.09.044

Thakur, R., Pristijono, P., Scarlett, C. J., Bowyer, M., Singh, S. P., & Vuong, Q. V. (2019). Starch-based films: Major factors affecting their properties. *International Journal of Biological Macromolecules, 132*, 1079–1089. https://doi.org/10.1016/j.ijbiomac.2019.03.190

Uranga, J., Nguyen, B. T., Si, T. T., Guerrero, P., & De la Caba, K. (2020). The effect of cross-linking with citric acid on the properties of agar/fish gelatin films. *Polymers, 12*(2). https://doi.org/10.3390/polym12020291

Wahyuningsih, K., Iriani, E. S., & Fahma, F. (2016). Utilization of cellulose from pineapple leaf fibers as nanofiller in polyvinyl alcohol-based film. *Indonesian Journal of Chemistry, 16*(2), 181–189.

Wang, K., Wang, W., Ye, R., Liu, A., Xiao, J., Liu, Y., et al. (2017). Mechanical properties and solubility in water of corn starch-collagen composite films: Effect of starch type and concentrations. *Food Chemistry, 216*, 209–216. https://doi.org/10.1016/j.foodchem.2016.08.048

Wen, L., Liang, Y., Lin, Z., Xie, D., Zheng, Z., Xu, C., et al. (2021). Design of multifunctional food packaging films based on carboxymethyl chitosan/polyvinyl alcohol crosslinked network by using citric acid as crosslinker. *Polymer, 230*, Article 124048.

Wu, H., Lei, Y., Lu, J., Zhu, R., Xiao, D., Jiao, C., et al. (2019). Effect of citric acid induced crosslinking on the structure and properties of potato starch/chitosan composite films. *Food Hydrocolloids, 97*, Article 105208. https://doi.org/10.1016/j.foodhyd.2019.105208

Wu, Z., Wu, J., Peng, T., Li, Y., Lin, D., Xing, B., et al. (2017). Preparation and application of starch/polyvinyl alcohol/citric acid ternary blend antimicrobial functional food packaging films. *Polymers, 9*(3). https://doi.org/10.3390/polym9030102

Yurong, G., & Dapeng, L. (2020). Preparation and characterization of corn starch/PVA/glycerol composite films incorporated with ε-polylysine as a novel antimicrobial packaging material. *E-Polymers, 20*(1), 154–161.

Zhao, K., Wang, W., Teng, A., Zhang, K., Ma, Y., Duan, S., et al. (2020). Using cellulose nanofibers to reinforce polysaccharide films: Blending vs layer-by-layer casting. *Carbohydrate Polymers, 227*. https://doi.org/10.1016/j.carbpol.2019.115264